



MIT Open Access Articles

Edge radial electric field structure and its connections to H-mode confinement in Alcator C-Mod Plasmas

The MIT Faculty has made this article openly available. **Please share** how this access benefits you. Your story matters.

Citation	McDermott, R. M. et al. "Edge radial electric field structure and its connections to H-mode confinement in Alcator C-Mod plasmas." <i>Physics of Plasmas</i> 16.5 (2009): 056103-12. ©2009 American Institute of Physics.
As Published	http://dx.doi.org/10.1063/1.3080721
Publisher	American Institute of Physics
Version	Author's final manuscript
Accessed	Sat Feb 02 00:16:46 EST 2019
Citable Link	http://hdl.handle.net/1721.1/55957
Terms of Use	Article is made available in accordance with the publisher's policy and may be subject to US copyright law. Please refer to the publisher's site for terms of use.
Detailed Terms	

Edge radial electric field structure and its connections to H-mode confinement in Alcator C-Mod Plasmas

R. M. McDermott, B. Lipschultz, J. W. Hughes, P. J. Catto, A. E. Hubbard,
I. H. Hutchinson, R. S. Granetz, M. Greenwald, B. LaBombard, K. Marr,
M. L. Reinke, J. E. Rice, D. Whyte, and the Alcator C-Mod Team¹

¹*Plasma Science and Fusion Center,
Massachusetts Institute of Technology, 175 Albany Street,
Cambridge, Massachusetts, 02139, USA*

(Dated: May 16, 2009)

Abstract

High-resolution charge-exchange recombination spectroscopic measurements of B^{5+} ions have enabled the first spatially resolved calculations of the radial electric field (E_r) in the Alcator C-Mod pedestal region [E. S. Marmor, *Fusion Science and Technology* **51**, 261 (2006)]. These observations offer new challenges for theory and simulation, and provide for important comparisons with other devices. Qualitatively, the field structure observed on C-Mod is similar to that on other tokamaks. However, the narrow high confinement mode (H-mode) E_r well widths (5mm) observed on C-Mod suggest a scaling with machine size, while the observed depths (up to 300kV/m) are unprecedented. Due to the strong ion-electron thermal coupling in the C-Mod pedestal it is possible to infer information about the main ion population in this region. The results indicate that in H-mode the main ion pressure gradient is the dominant contributor to the E_r well and that the main ions have significant edge flow. C-Mod H-mode data show a clear correlation between deeper E_r wells, higher confinement plasmas, and higher electron temperature pedestal heights. However, improved L-mode (I-mode) plasmas exhibit energy confinement equivalent to that observed in similar H-mode discharges, but with significantly shallower E_r wells. I-mode plasmas are characterized by H-mode like energy barriers, but with L-mode like particle barriers. The decoupling of energy and particle barrier formation makes the I-mode an interesting regime for fusion research and provides for a low collisionality pedestal without edge localized modes (ELMs).

I. INTRODUCTION

It is commonly accepted that $\mathbf{E} \times \mathbf{B}$ velocity shear is responsible for the suppression of edge turbulence, which reduces the losses of both energy and particles across magnetic field lines and results in the formation of edge transport barriers and H-mode confinement[1–3]. However, the self consistent evolution of the radial electric field profile, pedestal shape, and improvement in plasma confinement are not well understood. Experimentally, it is clear that core plasma confinement is directly connected to, if not controlled by, the edge pedestal[4–8]. Plasma rotation and velocity shear are known to play an important role in the transition from L-mode to H-mode with the plasma spin up at the transition propagating from the plasma edge to the core[9, 10]. The source of this seemingly spontaneous rotation is unknown, though it may be connected to scrape off layer (SOL) flows, which couple across the last closed flux surface (LCFS)[11]. Measurements of flows and radial electric field behavior in the pedestal region may provide the missing link between the SOL and core observations. A better understanding of the role the radial electric field plays in pedestal physics should enable better control of edge transport and improve core plasma confinement. This is especially important since future fusion devices, like ITER[12], will require H-mode confinement to meet their operational goals.

On Alcator C-Mod a new pedestal charge exchange recombination spectroscopy (CXRS) diagnostic has been installed, which provides high resolution measurements of pedestal parameters and the radial electric field structure and behavior in a unique and relevant parameter regime. Most C-Mod discharges are free from any externally applied torque and operate at ITER-like magnetic fields ($\sim 5\text{T}$) and plasma pressures (1MPa). Additionally, at high density, the C-Mod pedestal has ITER-like opacity to neutrals and thermally equilibrated electrons and ions, conditions currently unique to C-Mod.

Experimental observations on many different tokamaks have demonstrated the existence of a specific temporal and radial structure to the edge radial electric field surrounding the L-H transition. In L-mode plasmas the radial electric field inside the LCFS is small in magnitude and exhibits very little shear. However, in H-mode plasmas a negative radial electric field well forms just inside the last closed flux surface (LCFS). On DIII-D[13], evolution of the radial electric field has been observed prior to the L-H transition, as measured through an increase in the edge impurity poloidal velocity in the electron diamagnetic direction[14, 15].

This is in keeping with the theory that ExB shear suppression is instrumental to the L-H transition.

The E_r well on DIII-D in standard ELM-y H-mode plasmas is typically between -15 to -25 kV/m deep[16], although wells as deep as -100kV/m have been observed in QH-modes[17]. For all types of H-modes and plasma parameters, the DIII-D E_r wells are consistently of order 1cm in width[16, 17]. ASDEX-Upgrade[18] also observes an E_r well of order -35 to -50kV/m deep, located in the pedestal region during H-mode operation[19]. Like DIII-D, little variation in the E_r well width is observed. JET[20–22], JFT-2M[23, 24], and MAST[25, 26] all report similar observations of E_r well formation during H-mode operation, although details of the E_r well structure vary from machine to machine. Previous work on C-Mod estimated the magnitude of the radial electric field based on the propagation speed of magnetic fluctuations and inferred values of E_r of up to 250kV/m; this magnitude was over four times larger than measurements made on other machines [27]. The first spatially resolved measurements of the radial electric field profile on C-Mod confirm the initial estimates and will be described in detail in this paper.

This paper is organized as follows: an introduction to the new pedestal CXRS diagnostic is given in Section II. This includes hardware, geometry, and a description of the data obtained from the diagnostic. Section III describes two of the H-mode regimes seen on C-Mod and the radial electric field behavior that is observed in each. In Section IV, information about the behavior of the main ion population in the pedestal region is inferred through the measured radial electric field profiles. Section V explores the relationship between the depth of the H-mode radial electric field, plasma confinement and edge plasma parameters, and a potential scaling of E_r well width with machine size is introduced. In Section VI the I-mode regime and the radial electric field structure observed in these plasmas are described. Section VII presents a comparison of I-mode and EDA H-mode E_r profiles and offers several possible mechanisms that could explain the observed phenomenology. The key findings and conclusions are summarized in Section VIII.

II. THE EDGE CXRS DIAGNOSTIC ON ALCATOR C-MOD

The standard method for obtaining radial electric field profiles in fusion plasmas is to calculate them through the radial force balance equation[28],

$$E_r = \frac{1}{n_i Z_i e} \frac{dP_i}{dr} - V_{\theta i} B_\phi + V_{\phi i} B_\theta. \quad (1)$$

In Eq. (1) the contributions from the Reynolds stress and the off diagonal terms in the pressure tensor have been ignored. Experimental measurements of the impurity ion distribution function indicate that it is Maxwellian, justifying the simplification of the stress tensor to the gradient of the pressure. The contribution to E_r from the Reynolds stress is assumed to be small, an assumption that is particularly valid for the impurity ion species. The three terms left that contribute to E_r are the diamagnetic ($\frac{1}{n_i Z_i e} \frac{dP_i}{dr}$), poloidal velocity ($V_{\theta i} B_\phi$), and toroidal velocity ($V_{\phi i} B_\theta$) contributions.

To calculate E_r accurately, one needs to know the toroidal and poloidal magnetic fields as well as the temperature, density, and toroidal and poloidal velocity for a single species in the plasma. The poloidal magnetic field is determined by the EFIT[29] reconstruction of the plasma and a new high spatial resolution CXRS diagnostic on C-Mod provides simultaneous measurements of the necessary profiles for the B^{5+} population in the edge pedestal region. The system measures the charge exchange enhancement to the intrinsic B^{4+} emission ($n=7-6$, $\lambda_0=4944.67\text{\AA}$) that results through the interaction of the diagnostic neutral beam (DNB) with the B^{5+} population in the plasma. All temperatures, densities, and velocities in this paper refer to the B^{5+} population unless otherwise specified.

The low-field side edge CXRS system on C-Mod consists of three periscopes: a beam-viewing toroidal periscope, a beam-viewing poloidal periscope and a background (non-beam viewing) poloidal periscope. All three of these periscopes have a 4 to 5 cm viewing range covering the entire pedestal region with 3mm radial resolution. In addition to these three there is also a toroidal periscope that images the high-field side pedestal region. This periscope utilizes a D_2 gas puff at the inner wall to make localized charge exchange measurements of the B^{5+} population. The views from this periscope, when mapped to the outer wall, have equivalent spatial resolution to that of the low field side periscopes and the temperature profiles derived from its spectra can be used to complement the outer wall profiles. The spectra from the edge CXRS periscopes are collected by means of two fixed-grating Kaiser spectrometers[30, 31] coupled to two Photonmax charge coupled device cameras[32]. The system is capable of handling up to 108 views and typically operates with 5ms integration time and a duty cycle of 6.4ms.

Due to the narrow C-Mod pedestal widths (2-8mm)[8, 33], 3mm radial resolution is

the minimum required to make meaningful measurements in the pedestal region. Fig. 1 shows example temperature, density and velocity profiles obtained from the new CXRS diagnostic during an EDA H-mode discharge and illustrates the radial resolution with which the measurements can be made. The B^{5+} temperature profile, shown in Fig. 1a, forms a clear pedestal in H-mode and typically agrees well with the measured electron temperature pedestal. This is different from observations made on DIII-D, in which the impurity ion temperature pedestal is found to be wider than the electron temperature pedestal[7]. The H-mode B^{5+} density tends to be of order 1% of the electron density and also forms a clear pedestal in H-mode plasmas (Fig. 1b). The B^{5+} toroidal velocity is co-current in H-mode, consistent with what is observed in the core[9]. The B^{5+} poloidal velocity tends to be small in magnitude except in the pedestal region where it forms a peak in the electron diamagnetic direction.

The analysis of the CXRS data does not take into account cross-section effects on the charge exchange spectra[34]. These effects can potentially shift and broaden the observed spectra as a result of the energy dependence of the effective emission rate for the transition being considered. The magnitudes of the resultant velocity shift and temperature increase were evaluated for the C-Mod CXRS system geometry (and expected temperature and velocity ranges) and were found to be negligible. The apparent temperature broadening is typically less than a few eV, and the apparent velocity shift is less than 0.5km/s. The effect of the ion gyro-orbit and finite lifetime of the transition on the measured poloidal velocities[35] has not been considered. This effect is proportional to the plasma temperature and in the cold C-Mod pedestal region ($0.1 \text{ keV} \lesssim T_e \lesssim 0.5\text{keV}$) it is assumed to be small [35].

The measured B^{5+} poloidal velocity profiles have been compared to neoclassical predictions[36]. It was found that the neoclassically predicted profiles are qualitatively very similar to the measured profiles. The Pfirsch-Schlüter formulation[37], which is appropriate for the mid-pedestal region where the maximum poloidal velocity is measured, predicts a poloidal velocity in the correct direction and of roughly the right magnitude. However, the predicted velocity peak widths are wider than the measured (by 50-100%) and the peak locations are typically displaced; the predicted poloidal velocity peak tends to be displaced radially outward from the measured peak by several millimeters.

In this paper toroidal velocities are defined in a top down view of C-Mod. Velocities

in the clockwise direction are considered positive (forward field, co-current direction) and counter clockwise flows are negative. Similarly, poloidal velocities that are vertically upward at the low field side (forward field, electron diamagnetic direction) are positive, and vertically downward velocities (forward field, ion diamagnetic direction) are considered negative. These conventions do not alter when the magnetic field and plasma current directions are switched. To calculate the radial electric field, the temperature and density profiles from the CXRS diagnostic are fit to a modified tanh function, which is then used in conjunction with the raw poloidal and toroidal velocity profiles in Eq. (1). The details of the tanh fitting function can be found in Eq. (1) of reference [38].

III. E_r BEHAVIOR IN H-MODE PLASMAS

A. EDA H-modes

Enhanced D-alpha (EDA) H-modes are the most common types of H-modes run on C-Mod[39, 40]. They are quiescent H-modes without ELMs characterized by increased particle transport through the edge relative to ELM-free H-modes. This increase in edge transport can be observed through the increase in D_α emission during the H-mode period as shown in Fig. 2a. The enhanced particle transport is associated with a quasi-coherent mode (QCM) observed on the density and magnetics fluctuations between 80 and 150kHz[40, 41]. The QCM develops shortly after the formation of the edge pedestals. It is localized to the electron density pedestal and is likely the result of a resistive ballooning instability. It is believed to be the density pedestal release mechanism that prevents impurities from accumulating in the core and increasing the radiated power. The increased particle transport allows for steady state H-mode operation with constant radiated power, density, temperature, and confinement. Fig. 2 shows the steady state nature of these parameters for a typical EDA H-mode. The QCM, and thus EDA H-modes, are only observed in high collisionality plasmas, typically $\nu^* > 1$ at the top of the pedestal, where ν^* is calculated according to

$$\nu^* = \frac{qR\nu_{ei}}{\epsilon^{\frac{3}{2}}v_{th,e}}. \quad (2)$$

Here, q is the local safety factor, R the major radius, ν_{ei} is the electron ion collision frequency, ϵ is the inverse aspect ratio, and $v_{th,e}$ is electron thermal velocity.

In EDA H-modes the radial electric field forms a deep negative well, relative to its L-mode values, within 10mm inside of the LCFS. The full width half maximum (FWHM) of the well has been observed to vary between 4 and 6mm. By examining the width of the well during steady state discharges we find it to be on average $5\text{mm} \pm 1.5\text{mm}$. However, it should be noted that the radial resolution of the diagnostic is approximately 3mm, and the E_r well could be narrower than the instrument's ability to discern. In EDA H-modes the depth of the E_r well is on average -75 kV/m deep, although wells as shallow as -30kV/m and as deep as -120 kV/m deep have been observed. At smaller minor radii the radial electric field is always positive and exhibits a smooth, slowly varying profile. Fig. 3(a) illustrates the general characteristics. Although variation in the E_r well depth has been observed on a shot to shot basis, the depth of the well in a given EDA H-mode is constant as a function of time. This is consistent with the steady-state nature of EDA H-modes. In Fig. 3(a) E_r profiles from several different time slices within a single EDA H-mode are plotted together to illustrate the temporal constancy of the E_r profile. The typical EDA E_r well yields an \mathbf{ExB} shearing rate of order $-3 \times 10^6 \text{Hz}$ as calculated via Eq. (3)[42].

$$\omega_{ExB} = \frac{r}{q(r)} \frac{d}{dr} \left(\frac{q(r)}{r} \frac{E}{B} \right) \quad (3)$$

As shown in Fig. 3(b) the shearing rate also remains constant in EDA H-modes.

Estimates of the growth rates of the instabilities in the C-Mod pedestal region were obtained from a stability analysis using GS2[43], a linear, electromagnetic, gyrokinetic stability code[44]. GS2 is a core stability code that assumes that the gradient scale length is much greater than the gyro radius and that the size of the fluctuations are small. These conditions are not well met in the C-Mod pedestal, however, these runs represent the best available estimates of the growth rates. The code was run using fully developed EDA H-mode temperature and density pedestal profiles and resulted in a maximum growth rate of order $5 \times 10^5 \text{Hz}$. This is similar in magnitude to the \mathbf{ExB} shearing rates observed in EDA H-modes. One should note that it is the L-mode instabilities that are theoretically suppressed by \mathbf{ExB} shear enabling the transition to H-mode, and that the growth rates of pressure driven instabilities in L-mode plasmas will be less than those calculated for fully developed H-mode pedestal profiles. However, after the transition the instabilities must remain suppressed if the plasma is to remain in H-mode. Therefore, the comparison of the H-mode instability

growth rates to the H-mode $\mathbf{E} \times \mathbf{B}$ shear rate is appropriate.

Generally, the relative contributions to the E_r well from the three components in Eq. (1) are similar from one EDA discharge to another. Fig. 4 displays an example of the various component profiles. The toroidal velocity contribution acts as a fixed positive offset to E_r , while the well itself is determined primarily by the poloidal velocity and diamagnetic contributions. The contributions from the diamagnetic and poloidal velocity terms tend to align well in location leading to an additive well depth. The poloidal velocity well depth is typically greater than the diamagnetic depth and considerably narrower. As a result, the poloidal velocity contribution tends to set the E_r well width and the $\mathbf{E} \times \mathbf{B}$ shearing rate. Inside the pedestal region the positive radial electric field is contributed to by a combination of co-current toroidal rotation and slightly ion diamagnetic poloidal flow. These two contributions far outweigh the slightly negative contribution from the diamagnetic component. In the core of the plasma the radial electric field remains positive as a result of co-current toroidal rotation, which is by far the dominant contribution. From these results it is clear that it is important to measure all three components in Eq. (1) in order to calculate the radial electric field correctly.

B. ELM-free H-modes

ELM-free H-modes are inherently transient and are characterized by a strong particle transport barrier. This barrier results in impurity accumulation during the H-mode, which eventually causes its radiative collapse[8]. Plasma and impurity density increase monotonically during ELM-free H-modes, while T_e , T_i , and energy confinement peak early and then degrade as a result of the increasing radiated power. These characteristics are shown in Fig. 5. Edge L-mode density and magnetic fluctuations are sharply suppressed at the onset of ELM-free H-modes, while the residual fluctuations during the ELM-free H-mode are largely incoherent. ELM-free H-modes provide interesting cases for studying radial electric field behavior because of their inherently transient nature and continuously evolving plasma parameters.

The radial electric field well observed in the beginning of ELM-free H-modes can be significantly deeper (over -300kV/m) than the wells observed in EDA H-modes. This is consistent with the better plasma confinement observed in ELM-free H-modes relative to

EDAs. The best ELM-free H-modes can have energy confinement up to 30% higher than the best EDA H-modes and much higher particle confinement[27, 45]. The E_r well width, however, like the pedestal width, remains the same as in EDA H-modes within the error bars of the measurement ($\pm 1.5\text{mm}$). This leads to \mathbf{ExB} shearing rates in ELM-free H-modes of up to -1.8×10^7 Hz, over 5 times larger than the typical shearing rates observed in EDA H-mode discharges. The depth of the E_r well and the \mathbf{ExB} shearing rate are not constant during ELM-free H-modes. Instead, as shown in Fig. 6, they decrease as the H-mode evolves. The FWHM of the E_r wells shown in Fig. 6 remain constant at 4mm.

In ELM-free H-modes the particle transport barrier is too strong. It leads to the accumulation of impurities in the plasma core, which in turn increases the radiated power. As the radiated power approaches the input power, it cools the plasma, degrading the plasma energy confinement and decreasing the edge temperature pedestal height and gradient. The radial electric field and \mathbf{ExB} shearing rate decline in response to the changes in the temperature pedestal. These results indicate that \mathbf{ExB} shear is linked more strongly to the edge energy barrier than to the particle barrier. Also, an additional mechanism is needed to explain the observed particle transport in ELM-free H-modes; \mathbf{ExB} shear alone is insufficient.

All of the components that contribute to the radial electric field evolve during ELM-free H-modes. This is shown in Fig. 7. The decay of the E_r well depth is observed through the evolution of both the B^{5+} diamagnetic and poloidal velocity contributions, which decrease by 30 and 50%, respectively. The toroidal velocity in the pedestal region remains fixed over the entire duration of the ELM-free H-mode and thus does not contribute to the change. However, the toroidal velocity inside the pedestal region decreases as the plasma confinement degrades as shown in Fig. 7(c). This is consistent with prior observations of intrinsic toroidal rotation on C-Mod tracking with plasma energy confinement[46]. The measured impurity poloidal velocity and the gradient of the electron temperature pedestal both show similar rates of decay during ELM-free H-modes. This is not surprising since neo-classically, poloidal impurity flows are driven, in part, by edge temperature gradients[37, 47, 48].

IV. COMPARISON TO MAIN ION E_r ESTIMATES

Impurity ion profiles are employed to calculate E_r due to the relative ease with which they can be measured. However, impurity profiles are not necessarily representative of the main

ion population, which controls the plasma dynamics and is thus the real species of interest. Since the radial electric field is the same for all species, information about the main ion population can be inferred by comparing the total radial electric field to an estimate of the main ion diamagnetic contribution. The difference between E_r and the main ion diamagnetic contribution provides a measure of the main ion flow perpendicular to the magnetic field, which is useful for comparing to theoretical predictions of main ion velocities. Additionally, this comparison can potentially yield information about the source or formation physics of the radial electric field as well as suggesting guidelines for creating self-consistent radial electric field profiles for modeling codes.

In the C-Mod pedestal the main ions and the B^{5+} impurity population are thermally very well coupled. Typical thermal equilibration times for the two species in EDA H-modes are between 1 and $5\mu s$, while local transport time scales are much longer, between 0.1 and 1ms. Therefore the B^{5+} temperature profiles are highly representative of the main ions. Experimentally, we observe good agreement between the B^{5+} and the electron temperature profiles as measured by the millimeter resolution edge Thomson scattering system[49]. From this, one can conclude that the edge electron temperature profiles are good estimates of the main ion temperature profiles. Additionally, by invoking quasi-neutrality, the main ion density profiles can be represented by the electron density profiles (also from the edge Thomson scattering system). Here the effect of Z_{eff} (~ 1.5) on the ion density has not been taken into account as it does not affect the pressure gradient.

Together the edge n_e and T_e profiles can be used to estimate the main ion diamagnetic contribution to E_r . This estimate can then be compared to the total radial electric field profile, as measured through the B^{5+} ions. During EDA H-modes it is possible to obtain high resolution, low noise, E_r profiles by averaging over the steady state portion of the discharge. As shown in Fig. 8, this method can illustrate the full shape and depth of the E_r profile and facilitate the comparison to the main ion diamagnetic contribution.

From Fig. 8 one can also see that the main ion diamagnetic contribution is similar in shape, depth, and position to the total radial electric field well, but is offset by 30-40 kV/m. These similarities indicate that the main ion pressure gradient is the dominant contributor to the radial electric field well in H-mode plasmas[50]. However, to satisfy the main ion radial force balance equation, Eq. (1), the difference between the total radial electric field and the main ion diamagnetic term must be realized by main ion rotation perpendicular to the

magnetic field. This can be seen by rearranging Eqn.(1) and solving for the perpendicular velocity,

$$\vec{V}_{\perp i} = -\frac{\vec{B}}{B^2} \times \left(E_r - \frac{\nabla_r P_i}{n_i Z_i e} \right) \hat{r}. \quad (4)$$

From this the main ion perpendicular flow is inferred to be of order -10km/s as shown in Fig. 9. One should note that the radial alignment of the main ion diamagnetic estimate from the Thomson data with respect to the radial electric field from CXRS data is subject to calibration errors in both systems as well as flux surface mapping uncertainties. These radial uncertainties are of order ± 2 mm and can have dramatic effects upon the shape, if not the magnitude, of the inferred main ion perpendicular velocities. The dashed lines in Fig. 9 indicate the changes to the main ion perpendicular flow profile that result if the alignment between the Thomson and CXRS data is shifted by 1mm in either direction. It is not possible to break down the main ion perpendicular rotation into toroidal and poloidal flows without making an assumption about the main ion flow parallel to the magnetic field. It is also possible to compare E_r to the electron diamagnetic contribution and infer information about the electron flows in the pedestal region. This comparison gives an electron perpendicular flow velocity of order 40km/s in the pedestal region. This is expected as the electrons must speed up to satisfy $J \times B = \nabla P$.

V. SCALING OF E_r WITH PLASMA CONFINEMENT

The relationship between the depth of the radial electric field well and plasma energy confinement has been explored and a clear correlation found between deeper H-mode radial electric field wells and higher energy confinement plasmas. This correlation is shown in Fig. 10 and is in keeping with the paradigm of $\mathbf{E} \times \mathbf{B}$ shear suppression as the mechanism by which pedestals form and H-mode confinement is achieved. Within this framework, deeper E_r wells provide stronger $\mathbf{E} \times \mathbf{B}$ shear, which gives an increased capacity for turbulence suppression, leading to higher pedestal heights and improved plasma confinement, as a result of stiff core T_i profiles.

The depth of the radial electric field is also correlated with local pedestal parameters. In Fig. 11 the E_r well depth is shown as a function of electron pedestal density, temperature, and pressure at the top of the pedestal. There exists a weak correlation between the well

depth and pedestal density, but a much stronger correlation with the pedestal temperature, and as a result the pedestal pressure. These results reinforce the observations made in ELM-free H-modes, that particle confinement and energy confinement are controlled by different physical mechanisms. However, as H-mode density and temperature pedestals are observed to form simultaneously, the mechanisms are likely linked. The correlation between deeper radial electric field wells and higher pedestal pressure heights is in keeping with the main ion diamagnetic term being the dominant contribution to E_r .

The narrow E_r well width on C-Mod, as compared to the widths measured on other devices, suggests a scaling of E_r well width with machine size. One expects this trend if the main ion pressure gradient is the dominant term setting the E_r well, since H-mode pedestal width also scales roughly with machine size. As can be seen in Fig. 12, the published radial electric field structure data from several different devices[16, 17, 21, 24], with the exception of the JFT-2M data point, supports this supposition. These E_r well widths were obtained by fitting the data from these machines to a single Gaussian plus a polynomial background, which for the most part represented the data well. The JFT-2M data, which was published in 1990, was not well represented by a single Gaussian. However, even by simple inspection the FWHM of this well is of order 2cm, which does not support the trend created by the other machines.

VI. E_r BEHAVIOR IN IMPROVED L-MODE

On C-Mod typical transitions between L-mode and H-mode occur on a sub-millisecond time scale. This is too fast to capture the dynamics of the edge radial electric field with the current CXRS diagnostic system. However, discharges in the unfavorable ion $B \times \nabla B$ drift direction with input power just below the H-mode threshold can evolve more slowly towards L-H transitions, providing a potential tool for studying and understanding L-H transition dynamics. This slow evolution has been observed previously on both C-Mod and ASDEX Upgrade[4, 51, 52], but always as transient phenomena[52]. Recent experiments on C-Mod have developed this transient period into a steady state operational regime that can persist for many energy confinement times. This regime is characterized by an L-mode like edge particle barrier, but an H-mode like energy barrier, and has been termed an 'Improved L-mode', or 'I-mode'.

In I-mode the plasma density increases modestly coincident with the application of ion cyclotron resonant heating (ICRH) power, but does not increase further or approach its H-mode values. The plasma temperature, however, approaches and maintains its full H-mode value during the I-mode period. These features can be seen in the core plasma traces shown in Fig. 13. Here, the I-mode portion of the discharge, highlighted in gray, persists for 400ms and ends when the plasma transitions into an ELM-free H-mode at 1.2s. The key differences between L-, I-, and H-mode plasmas are illustrated in Fig. 14, which displays the edge electron temperature and density pedestals in these regimes. Here, the I-mode electron temperature pedestal approaches a full H-mode pedestal, while the electron density pedestal remains significantly closer to its L-mode levels. Similar behavior is observed in the corresponding B^{5+} temperature and density pedestal profiles.

The I-mode evolves smoothly from L-mode plasmas after the application of ICRH power; there is no apparent bifurcation or clear transition point. Although the I-mode appears to be an intermediate state between L-mode and H-mode, the transition from I-mode to H-mode remains an apparent bifurcation, only after which an H-mode density pedestal forms. During I-mode, H-mode like plasma confinement ($H98 = 0.8$) is maintained concomitant with H-mode like plasma temperature Fig. 13(d-e). The improved confinement can be maintained in steady state, due to the L-mode like particle confinement, which prevents the buildup of impurities and consequently the increase in radiated power. The steady state operation in I-mode is associated with an edge turbulence mode observed on the density and magnetic fluctuations around 100kHz as shown in Fig. 13 (f). The mode appears to be similar to the QCM observed in EDA H-mode operation, but exists at much lower collisionality ($\nu^* < 1$) and is spread over a wider frequency range.

The radial electric field in I-mode plasmas is qualitatively similar to that observed in EDA H-modes, but smaller in magnitude as can be seen in Fig. 15. The I-mode E_r well is between 15 and 30 kV/m deep and forms at the edge of the plasma within 10mm inside of the LCFS. The width of the well remains roughly 5mm leading to \mathbf{ExB} shearing rates between 0.5 and 2MHz. This is less than typical EDA \mathbf{ExB} shearing rates. In keeping with the \mathbf{ExB} shear suppression theory, it is possible that in improved L-mode plasmas the level of \mathbf{ExB} shear attained is approaching, but still less than, the critical value needed to suppress the edge turbulence effectively and initiate the transition to H-mode.

In I-mode plasmas all three components in Eq. (1) contribute to the E_r well structure.

This is different than in the H-mode plasmas, in which the toroidal velocity component acted as a fixed offset only. In I-mode, the toroidal velocity decreases in the counter-current direction instead of increasing in the co-current direction as it does in H-mode. This decrease acts to increase the E_r well depth and the \mathbf{ExB} shear rate. The counter current toroidal rotation is potentially connected to the observed turbulence mode and may be critical to understanding the I-mode transport.

VII. COMPARISON OF I-MODE TO EDA H-MODE

I-modes and EDA H-modes represent two steady state, high energy confinement regimes that are free from ELMs and exist in very different collisionality regimes. I-modes and EDA H-modes with similar L-mode parameters, including plasma shape, density, and input power can be compared and it is found that the I-mode attains the same energy confinement (H98) as the EDA H-mode, but does so with only half the edge \mathbf{ExB} shear (Fig. 15). This is consistent with the ELM-free H-mode result that the control mechanism for plasma energy transport is separate from the particle transport. However, it is inconsistent with the observed H-mode correlation between improved energy confinement and increased \mathbf{ExB} shear.

As I-modes are only observed in discharges with the X-point in the unfavorable drift direction, this suggests that doing so alters edge conditions such that the particle and energy transport can be decoupled. The mechanism by which this happens is unknown. It is possible that operating in the unfavorable drift direction changes the dominant instability at the edge or alters the phase correlation between the density, temperature, and potential fluctuations[53] resulting in modified energy and particle transport. This could potentially occur as a result of changes in edge magnetic shear, SOL flows[11], or flows of the edge turbulent density fluctuations[54]. Alternatively, given that \mathbf{ExB} shear is more effective at longer wavelengths, the observed I-mode transport could be explained if, in the unfavorable drift direction, the radial edge turbulent energy flux peaked at a higher poloidal wave number than the particle flux. In this case the same \mathbf{ExB} shear would affect the two fluxes differently.

VIII. CONCLUSIONS

A new high resolution CXRS system measuring B^{5+} ions has enabled the determination of the radial electric field in the C-Mod edge pedestal with 3mm spatial resolution and 5ms temporal resolution. During H-mode operation, the radial electric field is positive in the core, but forms a negative well up to -300kV/m deep in the region 10mm inside of the LCFS. The well is consistently $5\text{mm} \pm 1.5\text{mm}$ in width regardless of type of H-mode or plasma parameters. This well is largely determined by the poloidal velocity and diamagnetic contributions in the B^{5+} radial force balance equation. The poloidal velocity contribution is typically the larger and narrower contribution of the two and dominates both the E_r well width and the \mathbf{ExB} shear. In determining E_r from B^{5+} measurements it is essential to measure accurately all three terms in the force balance equation.

On C-Mod the strong ion-electron thermal coupling allows the use of the electron temperature and density profiles to estimate the main ion diamagnetic contribution to the total radial electric field. The comparison of this estimate to E_r shows striking similarities in shape, location and well depth between the two, indicating that in H-modes the main ion pressure gradient makes the dominant contribution to the radial electric field. In addition, the offset in magnitude between the main ion diamagnetic term and the total electric field indicates that the main ions cannot be stationary at the edge; they must have a significant flow component perpendicular to the magnetic field.

C-Mod data clearly show a correlation between deeper H-mode radial electric field wells, higher confinement plasmas and higher $T_{e,ped}$ and $P_{e,ped}$ heights, consistent with \mathbf{ExB} shear suppression theory and the main ion pressure gradient term being the dominant H-mode contributor. In I-mode plasmas, however, it is possible to obtain significantly improved energy confinement with less \mathbf{ExB} shear than is required in H-mode operation. The E_r measurements in ELM-free H-modes and I-modes indicate that the control mechanisms for particle and energy transport, although likely connected, are separate, and \mathbf{ExB} shear alone is insufficient to explain all of the observed phenomenology.

ACKNOWLEDGMENTS

The authors would like to acknowledge the work and contributions of the entire C-Mod team, especially the operations, DNB and RF groups without whom this work would not have been possible. Additionally, many thanks to D. Ernst, R. Bell, R. Groebner, H. Yuh, and S. Zweben for many useful conversations, as well as their support and ideas. This work was supported by United States Department of Energy Cooperative Agreement Number DE-FC02-99ER54512

-
- [1] H. Biglari, P. H. Diamond, P. W. Terry, *Phys. Fluids B* **2**, 1 (1990).
 - [2] K. H. Burrell, *Phys. Plasmas* **4**, 1499 (1997).
 - [3] P. W. Terry, *Rev. Mod. Phys.* **72**, 109 (2000).
 - [4] M. Greenwald, R. L. Boivin, F. Bombarda, P. Bonoli, C. L. Fiore, D. Garnier, J. A. Goetz, S. N. Golovato, M. A. Graf, R. S. Granetz, S. Horne, A. Hubbard, I.H. Hutchinson, J.H. Irby, B. LaBombard, B. Lipschultz, E.S. Marmor, M.J. May, G.M. McCracken, P. O’Shea, J.E. Rice, J. Schachter, J.A. Snipes, P.C. Stek, Y. Takase, J.L. Terry, Y. Wang, R. Watterson, B. Welch and S.M. Wolfe, *Nucl. Fusion* **37**, 793 (1997).
 - [5] F. Ryter, A. Stäbler, G. Tardini, *Fusion Sci. Technol* **44**, 618 (2003).
 - [6] Y. Kamada, T. Fujita, S. Ishida, M. Kikuchi, S. Ide, T. Takizuka, H. Shirai, Y. Koide, T. Fukuda, N. Hosogane, K. Tsuchiya, T. Hatae, H. Takenaga, M. Sato, H. Nakamura, O. Naito, N. Asakura, H. Kubo, S. Higashijima, Y. Miura, R. Yoshino, K. Shimizu, T. Ozeki, T. Hirayama, M. Mori, Y. Sakamoto, Y. Kawano, A. Isayama, K. Ushigusa, Y. Ikeda, H. Kimura, T. Fujii, T. Imai, M. Nagami, S. Takeji, T. Oikawa, T. Suzuki, T. Nakano, N. Oyama, S. Sakurai, S. Konoshima, T. Sugie, K. Tobita, T. Kondoh, H. Tamai, Y. Neyatani, A. Sakasai, Y. Kusama, K. Itami, M. Shimada, H. Ninomiya, H. Urano, *Fusion Sci. Technol.* **42**, 185 (2002).
 - [7] R. J. Groebner, T. H. Osborne, M. E. Fenstermacher, A. W. Leonard, M. A. Mahdavi, R. A. Moyer, L. W. Owen, G. D. Porter, P. B. Snyder, P.C. Stangeby, T. L. Rhodes, and N. S. Wolf, *Fusion Sci. Technol.* **48**, 1011 (2005).
 - [8] J. W. Hughes, A. E. Hubbard, D. A. Mossessian, B. LaBombard, T. M. Biewer, R. S. Granetz,

- M. Greenwald, I. H. Hutchinson, J. H. Irby, Y. Lin, E. S. Marmor, M. Porkolab, J. E. Rice, J. A. Snipes, J. L. Terry, S. Wolfe, K. Zhurovich, *Fusion Sci. Technol.* **51**, 317 (2006).
- [9] J. E. Rice, W. D. Lee, E. S. Marmor, P.T. Bonoli, R.S. Granetz, M. J. Greenwald, A.E. Hubbard, I. H. Hutchinson, J. H. Irby, Y. Lin, D. Mossessian, J.A. Snipes, S.M. Wolfe and S.J. Wukitch, *Nucl. Fusion* **44**, 379 (2004).
- [10] J. E. Rice, A. C. Ince-Cushman, M. L. Reinke, Y. Podpaly, M. J. Greenwald, B. LaBombard, E. S. Marmor, *Plasma Phys. Control. Fusion* **50**, 124042 (2008).
- [11] B. LaBombard, J.E. Rice, A. E. Hubbard, J. W. Hughes, M. Greenwald, J. Irby, Y. Lin, B. Lipschultz, E. S. Marmor, C. S. Pitcher, N. Smick, S.M. Wolfe, S.J. Wukitch, *Nucl. Fusion* **44**, 1047 (2004).
- [12] M. Shimada, D. J. Campbell, V. Mukhovatov, M. Fujiwara, N. Kirneva, K. Lackner, M. Nagami, V. D. Pustovitov, N. Uckan, and J. Wesley, *Nucl. Fusion* **47**, S1 (2007).
- [13] J. L. Luxon, T. C. Simonen, R. D. Stambaugh, *Fusion Sci. Technol.* **48**, 807 (2005).
- [14] R. J. Groebner, K. H. Burrell, R. P. Seraydarian, *Phys. Rev. Lett.* **64**, 3015 (1990).
- [15] K. H. Burrell, T. N. Carlstrom, S. Coda, E. J. Doyle, P. Gohil, R. J. Groebner, J. Kim, R. A. Moyer, W. A. Peebles, C. L. Rettig, T. L. Rhodes, and D. M. Thomas, *Plasma Phys. Control. Fusion* **38**, 1313 (1996).
- [16] P. Gohil, K. H. Burrell, T. N. Carlstrom, *Nucl. Fusion* **38**, 93 (1998).
- [17] K. H. Burrell, W. P. West, E. J. Doyle, M. E. Austin, J. S. deGrassie, P. Gohil, C. M. Greenfield, R. J. Groebner, R. Jayakumar, D. H. Kaplan, L. L. Lao, A. W. Leonard, M. A. Makowski, G. R. McKee, W. M. Solomon, D. M. Thomas, T. L. Rhodes, M. R. Wade, G. Wang, J. G. Watkins and L. Zeng, *Plasma Phys. Control. Fusion* **46**, A165 (2004).
- [18] A. Herrmann, O. Gruber, *Fusion Sci. Technol.* **44**, 569 (2003).
- [19] J. Schirmer, G. D. Conway, H. Zohm, W. Suttrop, *Nucl. Fusion* **46**, S780 (2006).
- [20] J. Jacquinet, M. Keilhacker, and P. Rebut, *Fusion Sci. Technol.* **53**, 866 (2008).
- [21] N. C. Hawkes, D. V. Bartlett, D. J. Campbell, N. Deliyannis, R. M. Gianella, P. J. Lomas, N. J. Peakcock, L. Porte, A. Rookes, and P. R. Thomas, *Plasma Phys. Control. Fusion* **38**, 1261 (1996).
- [22] Y. Andrew, N. C. Hawkes, T. Biewer, K. Crombe, D. Keeling, E. De La Luna, C. Giroud, A. Korotkov, A. Meigs, A. Murari, I. Nunes, R. Sartori, T. Tala, *EPL* **83**, 15003 (2008).
- [23] Y. Kusama, M. Yamamoto, *Fusion Sci. Technol.* **49**, 89 (2006).

- [24] K. Ida, T. Fujita, M. Mori, K. Hoshino, N. Suzuki, T. Yamauchi, Phys. Rev. Lett. **65**, 1364 (1990).
- [25] A. Sykes, R. J. Akers, L. C. Appel, E. R. Arends, P. G. Carolan, N. J. Conway, G. F. Counsell, G. Cunningham, A. Dnestrovskij, Yu. N. Dnestrovskij, A.R. Field, S.J. Fielding, M.P. Gryaznevich, S. Korsholm, E. Laird, R. Martin, M.P.S. Nightingale, C.M. Roach, M.R. Tournianski, M.J. Walsh, C.D. Warrick, H.R. Wilson, S. You, Nucl. Fusion **41**, 1423 (2001).
- [26] H. Meyer, C. Bunting, P. G. Carolan, N. J. Conway, M. R. Dunstan, A. Kirk, R. Scannell, D. Temple, M. Walsh, Journal of Physics Conference Series **123**, 012005 (2008).
- [27] I. H. Hutchinson, R. S. Granetz, A. Hubbard, J. A. Snipes, T. Sunn Pedersen, M. Greenwald, B. LaBombard, Plasma Phys. Control Fusion **41**, A609 (1999).
- [28] K. Ida, Plasma Phys. Control. Fusion **40**, 1429 (1998).
- [29] L. L. Lau, H. St. John, R.D. Stambaugh, A.G. Kellman, and W. Pfeiffer, Nucl. Fusion **25**, 1611 (1985).
- [30] R. E. Bell, Rev. of Sci. Instrum. **75**, 4158 (2004).
- [31] Kaiser Optical Systems Inc., Ann Arbor, MI. <http://www.kosi.com>.
- [32] Princeton Instruments, www.princetoninstruments.com.
- [33] J. W. Hughes, D. A. Mossessian, A.E. Hubbard, B. LaBombard, E. S. Marmor, Phys. Plasmas **9**, 3019 (2002).
- [34] M. von Hellermann, P. Breger, J. Frieling, R. König, W. Mandl, A. Mass, and H. P. Summers, Plasma Phys. Control. Fusion **37**, 71 (1995).
- [35] R. E. Bell and E. J. Synakowski, Ann. Isr. Phys. Soc. **547**, 39 (2000).
- [36] K. Marr, B. Lipschultz, R. M. McDermott, P. Catto, A. Simakov, Comparison of neoclassical flow theory with CXRS measurements for the H-mode pedestal on Alcator C-Mo American Physical Society, 50th Annual Meeting of the APS Division of Plasma Physics (2008).
- [37] P. J. Catto and A. N. Simakov, Phys. Plasmas **13**, 052507 (2006).
- [38] J. W. Hughes, B. LaBombard, D. A. Mossessian, A.E. Hubbard, J. Terry, T. Biewer, Phys. Plasmas **13**, 056103 (2006).
- [39] M. Greenwald, R. Boivin, P. Bonoli, C. Fiore, J. Goetz, R. Granetz, A. Hubbard, I. H. Hutchinson, J. Irby, Y. Lin, E. Marmor, A. Mazurenko, D. Mossessian, T. Sunn Pedersen, J. Rice, J. Snipes, J. Terry, S. Wolfe and S. Wukitch, Plasma Phys. Control. Fusion **42**, A263 (2000).

- [40] M. Greenwald, R. Boivin, P. Bonoli, R. Budny, C. Fiore, J. Goetz, R. Granetz, A. Hubbard, I. Hutchinson, J. Irby, B. LaBombard, Y. Lin, B. Lipschultz, E. Marmor, A. Mazurenko, D. Mossessian, T. Sunn Pedersen, C. S. Pitcher, M. Porkolab, J. Rice, W. Rowan, J. Snipes, G. Schilling, Y. Takase, J. Terry, S. Wolfe, J. Weaver, B. Welch, and S. Wukitch, *Phys. Plasmas* **6**, 1943 (1999).
- [41] J. L. Terry, N. P. Basse, I. Cziegler, M. Greenwald, O. Grulke, B. LaBombard, S. J. Zweben, E. M. Edlund, J. W. Hughes, L. Lin, Y. Lin, M. Porkolab, M. Sampsell, B. Veto and S.J. Wukitch, *Nucl. Fusion* **45**, 1321 (2005).
- [42] T. S. Hahm, *Phys. Plasmas* **1**, 2940 (1994).
- [43] W. Dorland, F. Jenko, M. Kotschenreuther, B. N. Rogers, *Phys. Rev. Lett.* **85**, 5579 (2000).
- [44] H. Yuh, M. Greenwald, T. Fredian, J. Stillerman, Stability Analysis of C-Mod with Gyrokinetic Code GS2, American Physical Society, 42nd Annual Meeting of the APS Division of Plasma Physics (2000).
- [45] M. Greenwald, N. Basse, P. Bonoli, R. Bravenec, E. Edlund, D. Ernst, C. Fiore, R. Granetz, A. Hubbard, J. W. Hughes, I. Hutchinson, J. Irby, B. LaBombard, L. Lin, Y. Lin, B. Lipschultz, E. Marmor, D. Mikkelsen, D. Mossessian, P. Phillips, M. Porkolab, J. Rice, W. Rowan, S. Scott, J. Snipes, J. Terry, S. Wolfe, S. Wukitch, K. Zhurovich, *Fusion Sci. Technol.* **51**, 266 (2005).
- [46] J. E. Rice, E. S. Marmor, P. T. Bonoli, R. S. Granetz, M. J. Greenwald, A. E. Hubbard, J. W. Hughes, I. H. Hutchinson, J. H. Irby, B. LaBombard, W. D. Lee, Y. Lin, D. Mossessian, J. A. Snipes, S. M. Wolfe, S. J. Wukitch, *Fusion Sci. Technol* **51**, 288 (2006).
- [47] Y. B. Kim, P. H. Diamond, R. J. Groebner, *Phys. Fluids B* **3**, 2050 (1991).
- [48] P. Helander, *Phys. Plasmas* **8**, 4700 (2001).
- [49] J. W. Hughes, D. Mossessian, A. Hubbard, E. S. Marmor, *Rev. of Sci. Instrum.* **72**, 1107 (2001).
- [50] G. Kagan and P. J. Catto, *Plasma Phys. Control. Fusion* **50**, 085010 (2008).
- [51] F. Ryter, W. Suttrop, B. Brüsehaber, M. Kaufmann, V. Mertens, H. Murmann, A. G. Peeters, J. Stober, J. Schweinzer, H. Zohm, *Plasma Phys. Control. Fusion* **40**, 725 (1998).
- [52] A. E. Hubbard, J. W. Hughes, I. O. Bespamyatnov, T. Biewer, I. Cziegler, B. LaBombard, Y. Lin, R. M. McDermott, J. E. Rice, W. L. Rowan, J. A. Snipes, J. L. Terry, S. M. Wolfe, and S. Wukitch, *Phys. Plasmas* **14**, 056109 (2007).

- [53] A. S. Ware, P. W. Terry, P. H. Diamond, and B. A. Carreras, *Plasma Phys. Control. Fusion* **38**, 1343 (1996).
- [54] C. Fenzi, G. R. McKee, R. J. Fonck, K. H. Burrell, T. N. Carlstrom, and R. J. Groebner, *Phys. of Plasmas* **12**, 062307 (2005).

FIGURE CAPTIONS

Figure 1 (Color online) Simultaneous high-confinement mode profiles of (a) temperature $T_{B^{5+}}$, (b) density $n_{B^{5+}}$, and (c) toroidal and poloidal velocity $v_{\phi, B^{5+}}$, $v_{\theta, B^{5+}}$ from the edge CXRS diagnostic. The solid curves are fits to the data using a modified tanh function defined in equation [1] of reference[38]. The gray boxes highlight the pedestal region for each parameter. The vertical dashed line indicates the position of the last closed flux surfaces .

Figure 2 (Color online) Characteristics of a C-Mod EDA H-mode. (a) D_{α} , (b) radiated power, (c) line averaged density, (d) electron temperature, (e) plasma confinement factor H98, (f) magnetic fluctuations, and (g) input ICRF power. The gray highlighted region indicates the H-mode portion of the discharge.

Figure 3 (Color online) Examples of radial electric field and \mathbf{ExB} shear profiles in EDA H-modes. (a) E_r forms a deep negative well just inside the LCFS in H-mode. (b) The \mathbf{ExB} shearing rate frequency is of order 3MHz in the pedestal region. (b) The L-mode profiles are shown by the solid black lines. The circle symbols indicate the H-mode profiles. The colored profiles (online) are individual time frames.

Figure 4 (Color online) Contributions of the three components from Eq. [1] to the radial electric field in an EDA H-mode. The poloidal velocity contribution dominates the width of the E_r well.

Figure 5 (Color online) Characteristics of a C-Mod ELM-free H-mode. (a) D_{α} , (b) radiated power, (c) line averaged density, (d) electron temperature, (e) plasma confinement factor H98, (f) magnetic fluctuations, and (g) input ICRF power. The gray highlighted regions indicate the H-mode portions of the discharge.

Figure 6 (Color online) Examples of evolving radial electric field and \mathbf{ExB} shear profiles in ELM-free H-modes. (a) The depth of the E_r well diminishes as the H-mode evolves. (b) The \mathbf{ExB} shear frequency also decays as the ELM-free H-mode evolves.

Figure 7 (Color online) Evolution of all three contributions from Eq. [1] to the radial electric field in an ELM-free H-mode. The (a) diamagnetic component, (b) poloidal velocity contribution, (c) and toroidal velocity contribution all diminish as the ELM-free H-mode evolves.

Figure 8 (Color online) Comparison of E_r , as measured using B^{5+} ions, to an estimate of the main ion diamagnetic contribution to E_r from the Thomson scattering diagnostic. The

main ion diamagnetic estimate can account for most of the shape, depth, and position of the E_r well.

Figure 9 (Color online) Main ion perpendicular velocity determined by the difference between the total radial electric field and the estimate of the main ion diamagnetic contribution. The main ions have a significant flow component perpendicular to the total magnetic field in the pedestal region.

Figure 10 (Color online) Plasma confinement (H89) versus E_r well depth for EDA and ELM-free H-modes. There is a correlation between deeper radial electric field wells and improved plasma energy confinement.

Figure 11 (Color online) Edge electron pedestal parameters, (a) $n_{e,Ped}$, (b) $T_{e,Ped}$, (c) $P_{e,Ped}$ as a function of E_r well depth. There is a correlation between deeper radial electric field wells and higher temperature pedestal heights. There is little correlation between E_r and density pedestal heights.

Figure 12 (Color online) Radial electric field well widths (FWHM) versus machine major radii collected from the published literature,[16, 17, 21, 24]. The width of the radial electric field well appears to scale, to first order, with machine size.

Figure 13 (Color online) Characteristics of a C-Mod I-mode plasma. (a) D_α , (b) radiated power, (c) line averaged density, (d) electron temperature, (e) plasma confinement factor H98, (f) magnetic fluctuations, and (g) input ICRF power. The gray highlighted region indicates the I-mode portion of the discharge.

Figure 14 (Color online) Comparison of (a) edge electron temperature and (b) electron density profiles between L-mode, I-mode and H-mode plasmas. The I-mode temperature profile approaches H-mode values, while the I-mode density profile remains closer to L-mode levels.

Figure 15 (Color online) Comparison of (a) the radial electric field and (b) the \mathbf{ExB} shear profiles between an L-mode, I-mode, and EDA H-mode. I-mode radial electric field well depths and \mathbf{ExB} shear rates are lower than their H-mode counterparts.

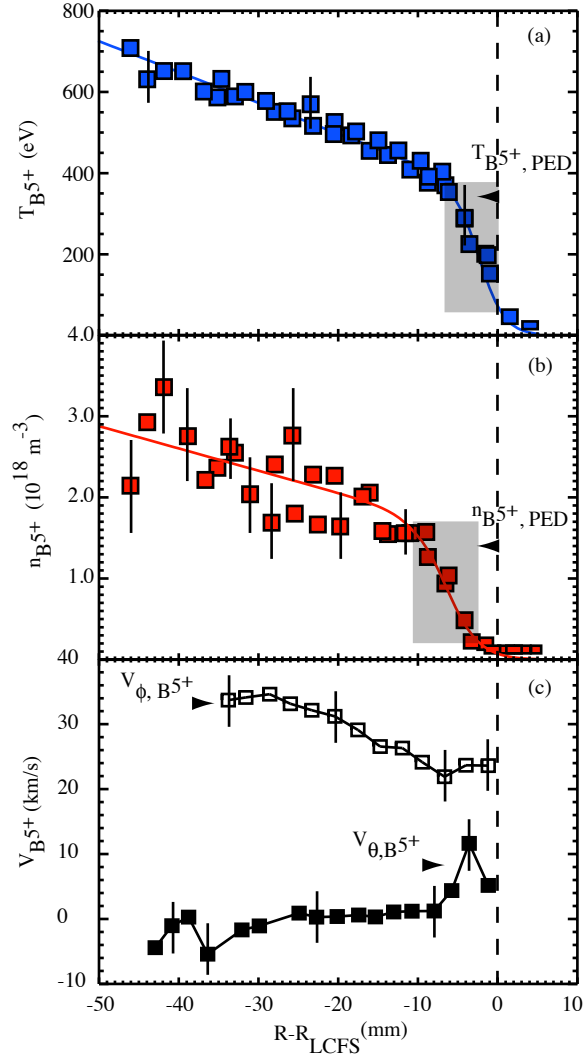


FIG. 1:

FIGURES

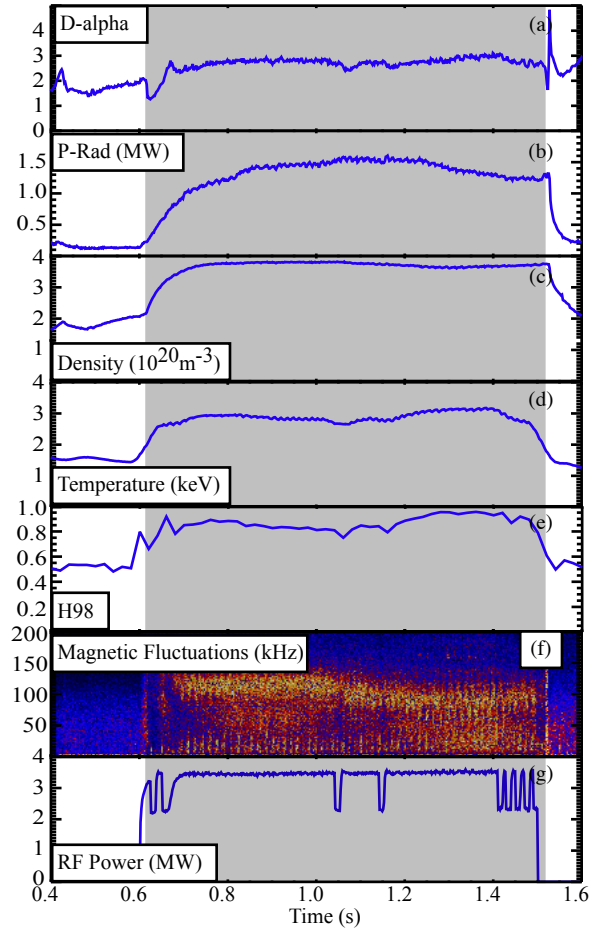


FIG. 2:

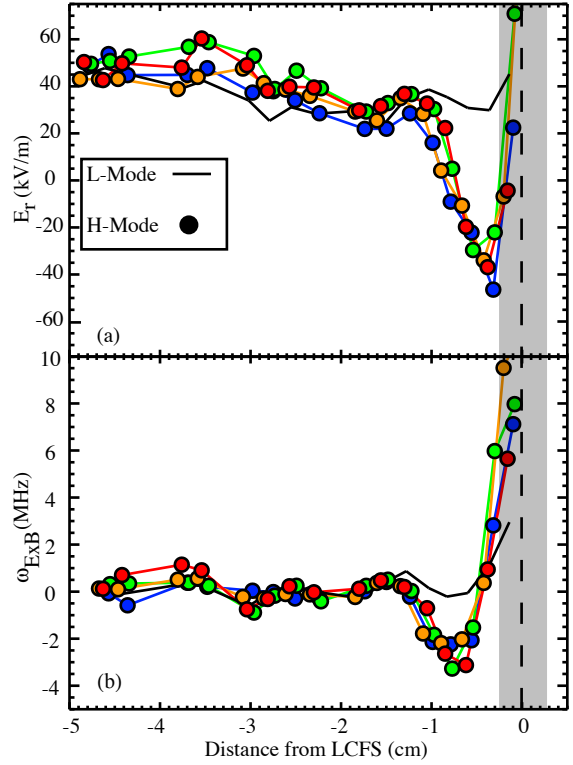


FIG. 3:

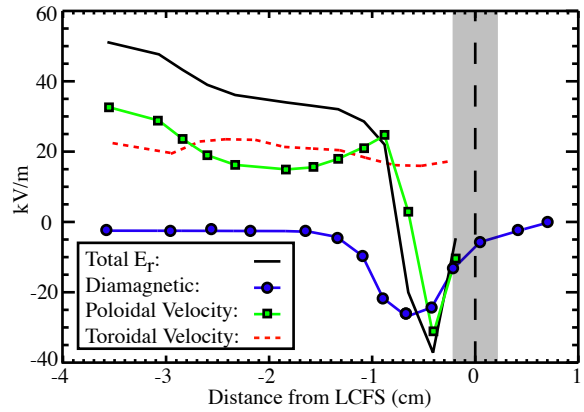


FIG. 4:

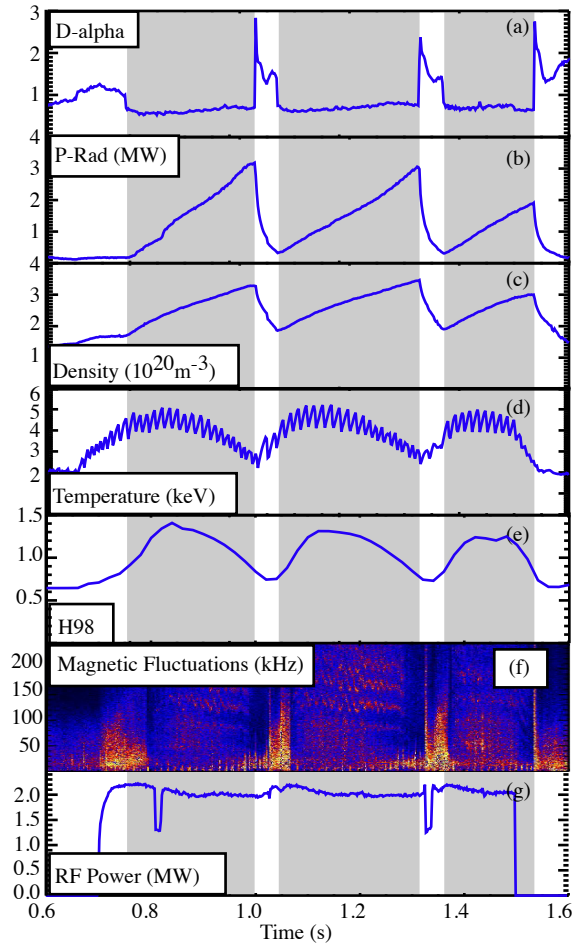


FIG. 5:

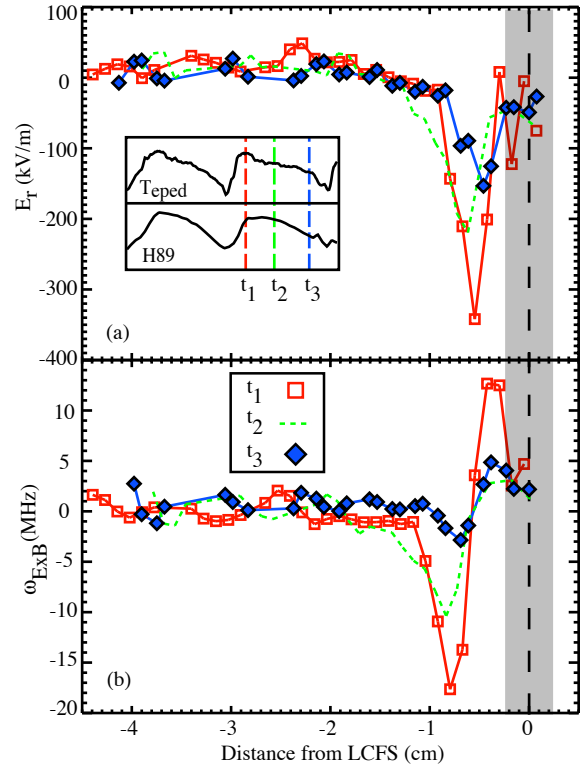


FIG. 6:

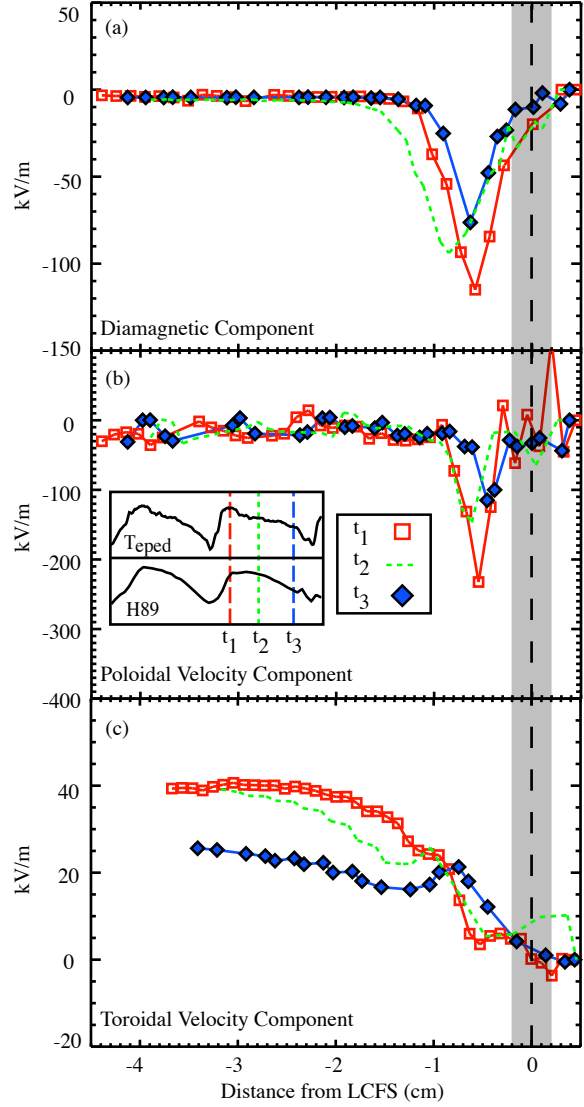


FIG. 7:

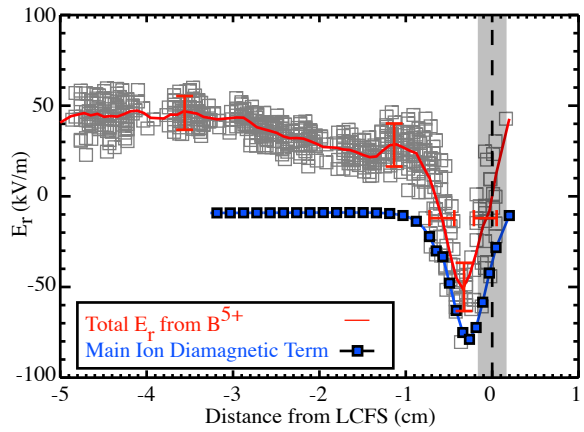


FIG. 8:

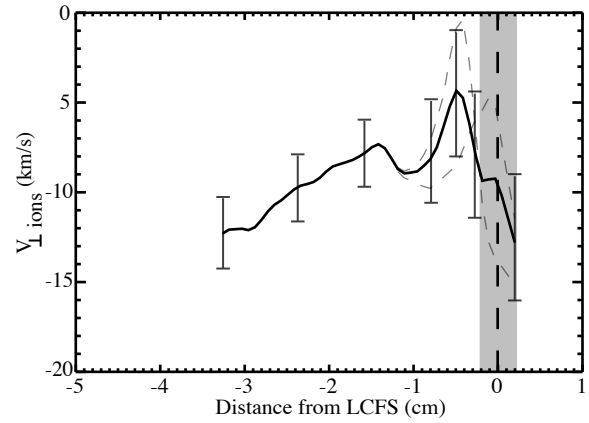


FIG. 9:

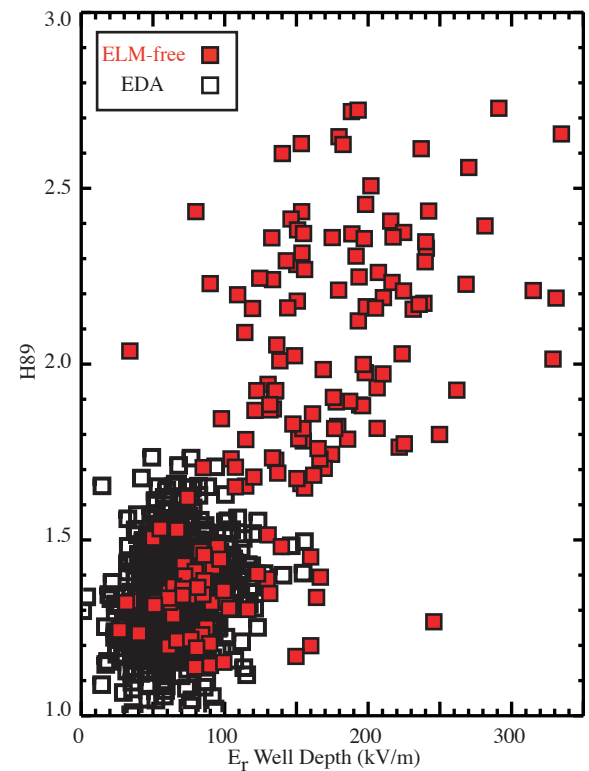


FIG. 10:

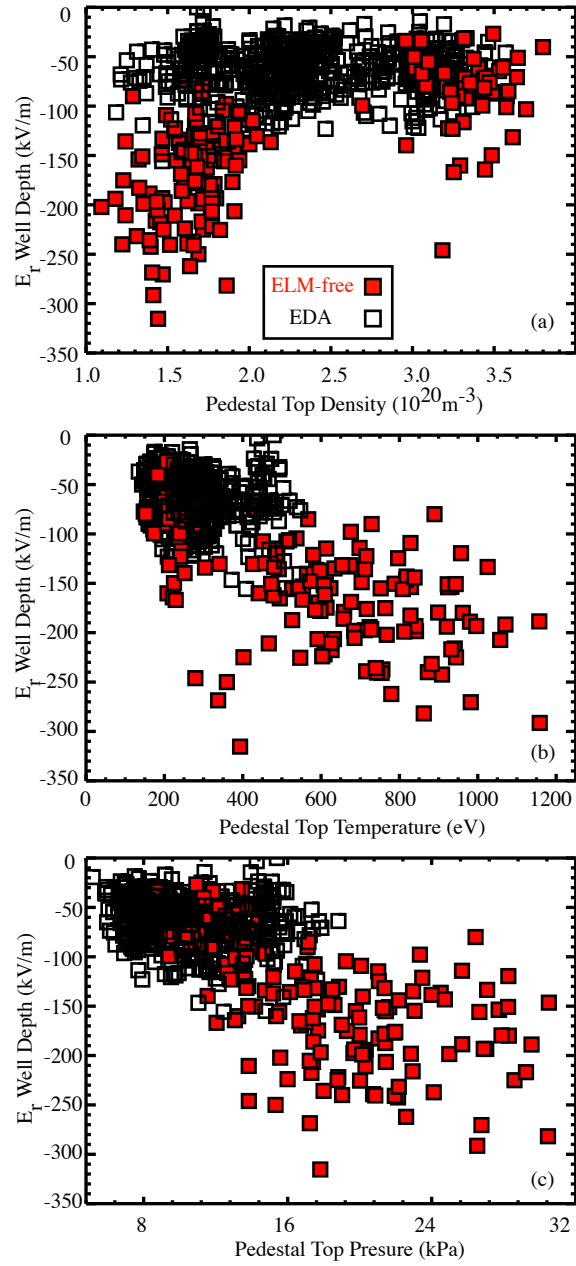


FIG. 11:

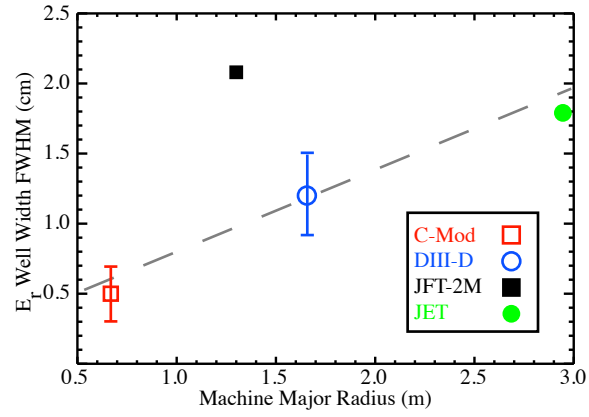


FIG. 12:

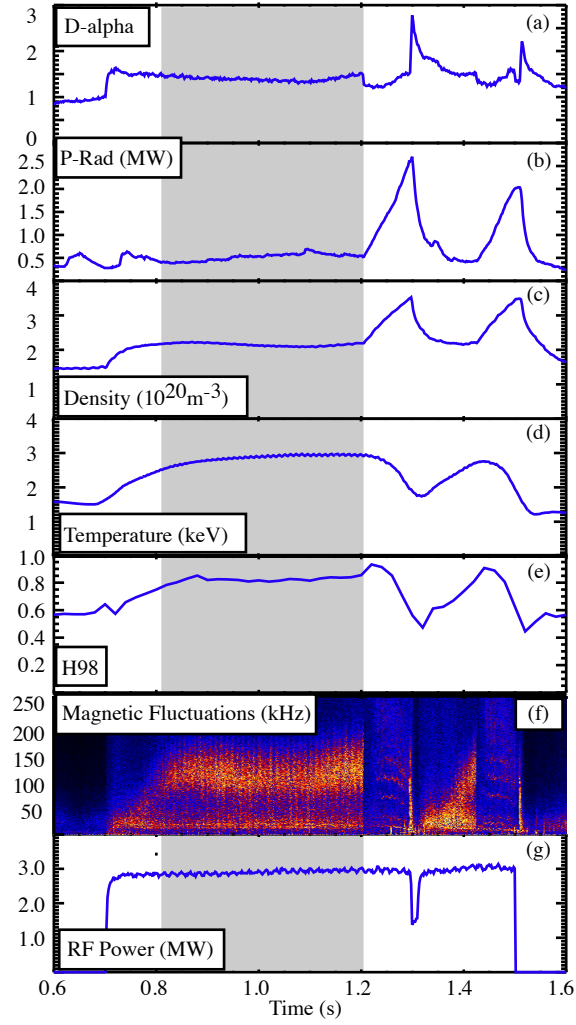


FIG. 13:

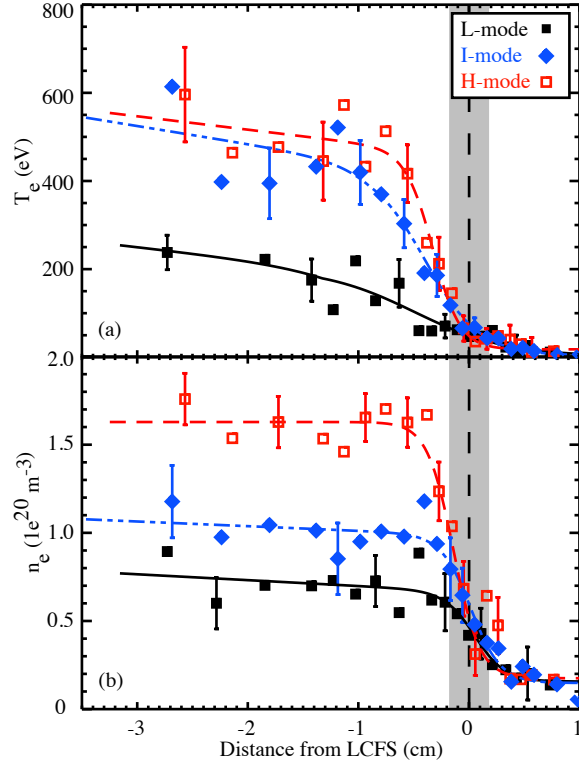


FIG. 14:

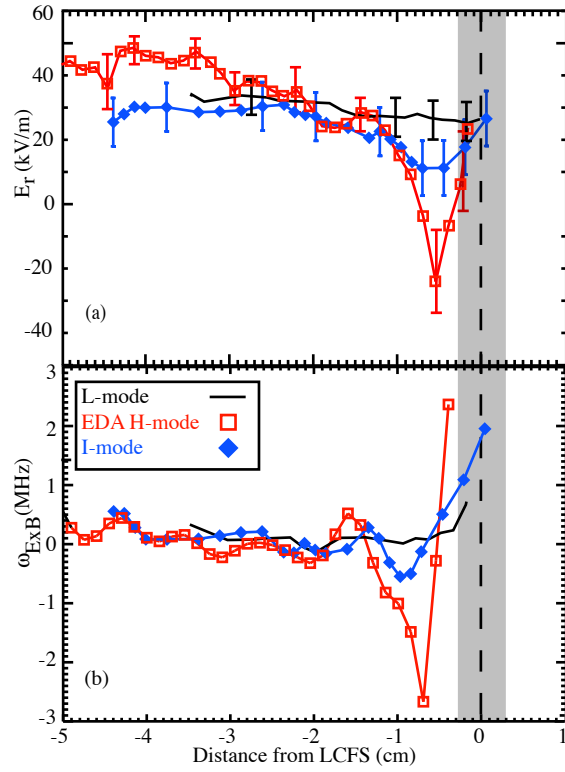


FIG. 15: